(Received 5 September 2025, Accepted 15 November 2025, Scheduled 23 November 2025)

Electrostatic Shielding of a Rectangular Conducting Enclosure: Influence of Aperture Position on the Penetrated Field

Xiaolin Zhao[1], Hanyu Wu[2], and Chongqing Jiao[2,*]

[1]China Electric Power Research Institute Co., Ltd., Haidian District, Beijing 100192, China
[2]State Key Laboratory of Alternate Electrical Power System with Renewable Energy Sources (North China Electric Power University), Changping District, Beijing 102206, China

ABSTRACT: This paper investigates, by means of finite-element simulations, how the position of an aperture affects the electrostatic shielding effectiveness of a rectangular metallic enclosure. First, we compute the electric-field distribution on the surface of a completely closed enclosure placed in an external electric field. The results show that, for every wall, the field is the weakest at the center and that the field on walls parallel to the external field is far lower than that on walls perpendicular to it. Next, we determine the electric field that leaks into the enclosure after an aperture is introduced. We find that the field strength decreases with the distance from the aperture, that the field near the aperture is proportional to the surface field at the aperture's location when the aperture is covered. Also, its magnitude can be predicted by the classical model of the small aperture coupling. Finally, we investigate the coexistence effect and formulate guidelines for choosing the aperture position to achieve optimum shielding performance.

1. INTRODUCTION

Electromagnetic shielding is the principal technical means of suppressing spatial and radiated electromagnetic disturbances [1]. Depending on the field source, it can be classified as electric-field shielding, magnetic-field shielding, or electromagnetic-wave shielding. For electric-field and electromagnetic-wave shielding, conductive enclosures are normally used to surround either the sensitive equipment or disturbance source. The electric field coupling is weakened through mechanisms such as electrostatic induction and eddy-current cancellation [2]. In contrast, shielding against low-frequency magnetic fields generally employs highly magnetically permeable materials, redirecting the magnetic flux to achieve the desired attenuation. In general, common metallic materials like copper and aluminum provide high shielding effectiveness (SE) against electric fields, electromagnetic waves, and magnetic fields at higher frequencies [3]. However, only metals with very high permeability — such as permalloy and iron-nickel alloys — can deliver substantial shielding against extremely low frequency or static magnetic fields. In practical applications, special requirements such as flexibility, light weight, transparency, and frequency selectivity have driven the design and development of a wide variety of shielding solutions, including frequency-selective surfaces [4], conformal shields [5], metamaterials, composite materials, and multilayer structures.

In addition to the choice of material, the presence of apertures is a key determinant of shielding effectiveness [6–9]. Practical considerations — ventilation, heat dissipation, cable routing — make openings unavoidable. Electromagnetic leakage through such apertures has long been a central topic in shielding research, and numerous publications address the theory, calculation methods, and characteristics of shielding effectiveness for enclosures with holes. Rather than reviewing this extensive literature, the present work focuses on the specific question of where to place an aperture in a rectangular enclosure for electrostatic shielding. This issue is of immediate practical importance, especially for enclosure designers: as power-system voltages rise and grids become more intelligent, high-voltage primary equipment and low-voltage secondary devices are increasingly co-located in compact arrangements. Such scenario exposes the latter to ever harsher electric-field disturbance.

Surprisingly, this fundamental question has received little attention in the literature; quantitative results are especially scarce. Refs. [10, 11] present an analytical theory — derived via separation of variables — for the shielding of a uniform external electrostatic field by a spherical shell containing a circular aperture. It shows that the shielding is strongest when the aperture is parallel to the applied field and weakest when it is perpendicular. In [12], two-dimensional axisymmetric problem — the penetration of an electric field through a nonuniform conducting cylindrical cavity with a slot is solved analytically. However, these studies do not address the rectangular enclosures that are far more common in practice. It should be noted that magnetic-field shielding is more intricate: the optimal aperture location depends on the prevailing mechanism. In eddy-current cancellation, for example, the aperture should be perpendicular to the external magnetic field [11], whereas in flux-shunting it should be parallel [13, 14]. For electromagnetic-wave shielding, a larger body of work exists; one representative example is [3], which develops an equivalent-circuit theory for computing the shielding effectiveness of a rectangular box against a plane

* Corresponding author: Chongqing Jiao (cqjiao@ncepu.edu.cn).

electromagnetic wave. The results again demonstrate that the best aperture location is dictated by the field distribution of the electromagnetic modes excited inside the cavity [15].

The rest of this article is organized as follows. In Section 2, the geometry configuration and finite element method (FEM) model are introduced. Section 3 investigates unperturbed surface E field, penetrated E field, the effect of aperture position, the choice of the aperture position, and the proximity effect between two adjacent apertures. Finally, Section 4 concludes this article. The main contributions are threefold. First, a comprehensive set of factors is examined, including over ten aperture positions, three enclosure shapes, more than one hundred observation points, and the coexistence effect. Second, concrete data and curves are provided, allowing a quantitative description of how aperture position affects the fields. Finaly, it is demonstrated that a simple analytical formula can satisfactorily predict the electric-field strength in the vicinity of an aperture.

2. MODEL

As illustrated in Figure 1, the rectangular enclosure is centered at the origin of the Cartesian coordinate system (X, Y, Z) and occupies the region $-l_x/2 \le x \le l_x/2$, $-l_y/2 \le y \le l_y/2$, $-l_z/2 \le z \le l_z/2$. To generate a uniform external electric field of 1 V/m in the x direction, we apply a potential of $+25$ V on the plane $x = -25$ m (-25 m $\le y \le 25$ m, -25 m $\le z \le 25$ m) and -25 V on the plane $x = 25$ m (-25 m $\le y \le 25$ m, -25 m $\le z \le 25$ m). In addition, the potential is assumed to decrease linearly with the increase of x on the four side planes: $y = -25$ m, $y = 25$ m, $z = -25$ m, and $z = 25$ m.

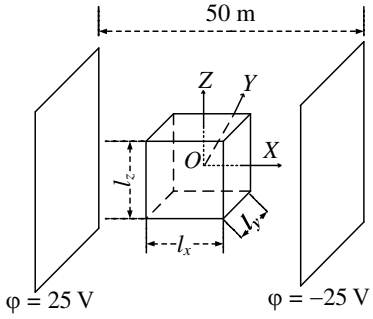

FIGURE 1. The configuration of the electrostatic Shielding problem: a shielding box with length, width, and height l_x, l_y, and l_z, respectively, is placed in an applied electrostatic field of 1 V/m.

In the following simulations, the enclosure dimensions do not exceed 0.4 m, which is much smaller than the dimensions of the excitation boundaries. Owing to the geometric and excitation symmetry of the entire model, assigning zero potential to the enclosure renders it electrically neutral. The aperture is assumed to be circular because, for a given area, a circular opening provides the best shielding effectiveness. The radius of the circular hole is always equal to 1 cm, which is far smaller than any side length of the enclosure. In practice, the material of the shielding boxes should be highly conductive, such as common metals like aluminum, steel, and copper.

The finite element model is built with the commercial COMSOL software [16]. Adaptive mesh refinement was used to ensure the convergence of the computational results. The 3-D model for this electrostatic shielding problem is built in the "electrostatics" solver of the AC/DC Module in the COMSOL software. We use a user-defined mesh for the region inside the shielding box and use a physics-defined mesh for the region outside the box. For the former, the maximum mesh size is 4 mm, and the minimum mesh size is 1 mm. For the latter, the mesh preset "fine" is applied. The selected element shape is free triangular. The maximum number of meshes is about 20 million. The total computation time is about 40 s to 80 s, with a person computer (Intel Core i9-14900HX (24-core), 5.2 GHz, and 64 GB RAM).

3. RESULTS AND DISCUSSIONS

3.1. The Unperturbed Surface *E* Field

Assume that the shielding box is a cube with edge length 0.4 m. Figures 2(a) and 2(b) show the magnitude distributions of the electric field on the surfaces perpendicular ($x = -0.2$ m, -0.19 m $< y, z < 0.19$ m) and parallel ($y = -0.2$ m, -0.16 m $< x, z < 0.16$ m) to the applied field, respectively. Note that the distribution on the wall at $x = 0.2$ m is similar to that at $x = -0.2$ m and thus is omitted. Likewise, the distributions on the remaining three faces are analogous to that on $y = -0.2$ and are also omitted.

As displayed in Figure 2(a), the electric-field strength exhibits both vertical and horizontal symmetry, reaching its minimum at the center of the wall. Near the center, the field contours are nearly circular; as the observation point moves away, the contours gradually become square. Figure 2(b) reveals a similar symmetry pattern, with the minimum field strength located along the central line ($x = 0$). By comparing the two figures, we find that the field on the wall perpendicular to the applied field (Figure 2(a)) is significantly stronger than that on the parallel wall (Figure 2(b)). This occurs because the perpendicular surface can accumulate more induced charges, whose density is especially high at the edges where the curvature is the greatest.

3.2. The Penetrated *E* Field

Ten aperture positions are selected on the wall at $x = -0.2$ m, as illustrated in Figure 3. The (y, z) coordinates of the centers of the apertures are: A (0 m, 0 m), B (0 m, 0.05 m), C (0.05 m, 0.05 m), D (0 m, 0.1 m), E (0.05 m, 0.1 m), F (0.1 m, 0.1 m), G (0 m, 0.15 m), H (0.05 m, 0.15 m), I (0.1 m, 0.15 m), and J (0.15 m, 0.15 m). Next, a circular aperture with radius 1 cm is opened individually at each of these ten points. For every aperture, 21 observation points are set along the normal line perpendicular to the aperture and passing through its center, as shown in Figure 4. Take the 21 observation points corresponding to the aperture A as an example, their y- and z-coordinates are identical to those of the center of aperture A, respectively. Their x-coordinates are evenly distributed between $x = -0.2$ m and $x = 0$ m.

Figure 5 presents the electric-field strengths at the 21 observation points for each of the aperture locations described above. To clearly display these field strengths, the 21 observation points are divided into three groups, shown in Figures

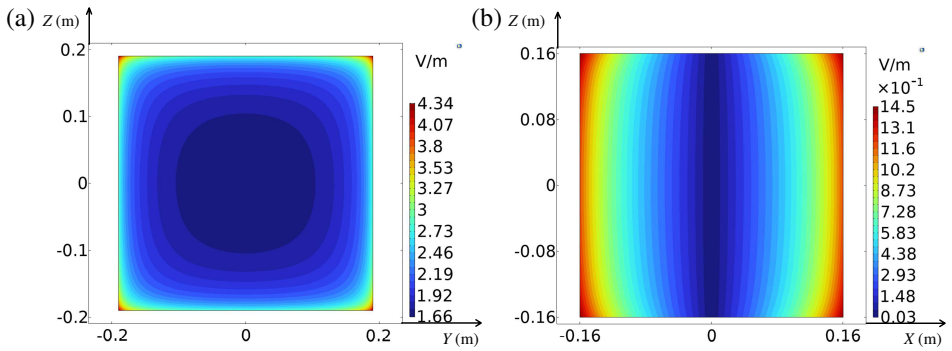

FIGURE 2. The electric-field distribution on the shielding-box surface: (a) surface at $x = -0.2$ m; (b) surface at $y = -0.2$ m.

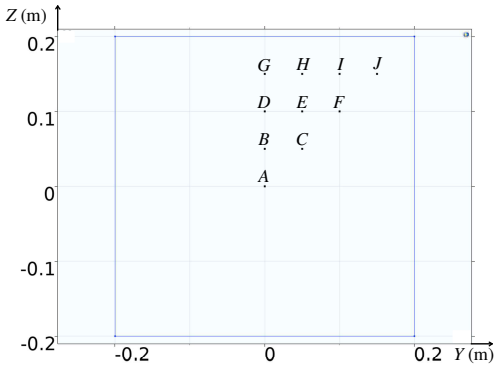

FIGURE 3. Ten aperture positions are selected on the wall at $x = -0.2$ m. Their (y, z) coordinates are A (0 m, 0 m), B (0 m, 0.05 m), C (0.05 m, 0.05 m), D (0 m, 0.1 m), E (0.05 m, 0.1 m), F (0.1 m, 0.1 m), G (0 m, 0.15 m), H (0.05 m, 0.15 m), I (0.1 m, 0.15 m), and J (0.15 m, 0.15 m).

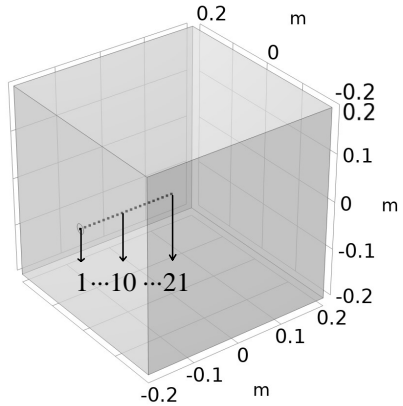

FIGURE 4. For each aperture position in Figure 3, 21 observation points are evenly distributed along the line perpendicular to the aperture plane. The observation point 1 is located at the center of the aperture. The distance between the observation points 21 and 1 equals half of the corresponding side length of the shielding box.

5(a), 5(b), and 5(c), respectively. Specifically, Figure 5(a) includes observation points 1 to 3; Figure 5(b) includes points 3 to 11; and Figure 5(c) includes points 11 to 21. In addition, the vertical axes in Figures 5(a) and 5(b) use linear scales, while that in Figure 5(c) uses a logarithmic (ratio) scale. It is evident that the field strength drops rapidly as the observation point recedes from the aperture center: the field at observation point 4 is less than 1% of that at point 1 (the aperture center). This indicates that when the distance from the field point to the aperture exceeds three times of the aperture radius, the field is attenuated by more than 40 dB. Moreover, the field strengths near the aperture obviously vary with aperture location. In general, the farther the aperture is from the wall center, the stronger the local field becomes; for instance, the field at location J is 1.35 times that at location A. It can also be observed that these curves intersect. Taking apertures A and J as an example: when the field points are close to the apertures, the field strength under aperture J is stronger than that under aperture A; when the field point is far away (observation points 15 to 21), the field strength under aperture J becomes weaker than that under aperture A.

In addition, we also computed the axial field distribution when a circular aperture is opened at the center of the side wall ($y = -0.2$ m), although not plotted here. The resulting field strengths range from 5.4×10^{-5} V/m to 6.6×10^{-7} V/m, which are orders of magnitude smaller than those obtained when the aperture is on the front wall ($x = -0.2$ m).

3.3. Effect of Aperture Position

First, for the ten aperture positions mentioned earlier, the unperturbed fields (i.e., the unperturbed fields before the apertures are introduced) are listed below: 1.66 V/m (A), 1.67 V/m (B), 1.69 V/m (C), 1.74 V/m (D), 1.76 V/m (E), 1.82 V/m (F), 1.94 V/m (G), 1.96 V/m (H), 2.02 V/m (I), 2.22 V/m (J). By comparing the field strengths at the center of the aperture before and after the opening, we find that the post-aperture electric field equals exactly one-half of the unperturbed value. It should be noted that this conclusion is rigorously valid for an aperture in an infinite plane, as pointed out by Jackson [17]. Here, although the shielding-box surface is not an infinite plane, the result still applies provided that the aperture dimensions are much smaller than the box edge length, and the aperture is not located near the edges of the box.

Electromagnetic leakage through electrically small apertures is a classic problem in electromagnetic theory and applications. It was first investigated systematically by Bethe [18], who showed that the electric and magnetic leakage fields can be represented, respectively, by an electric dipole and a magnetic dipole located at the center of the aperture. The electric dipole is oriented normal to the aperture plane, with its moment being proportional to the normal component of the external electric field. And the magnetic dipole lies in the tangent plane, with its

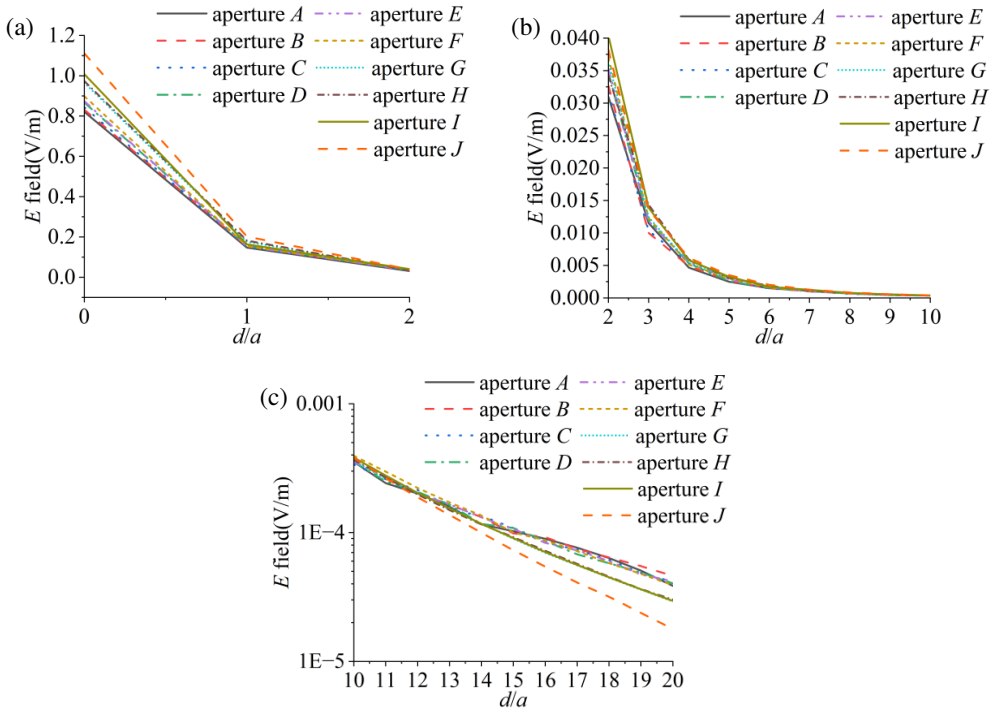

FIGURE 5. Electric-field distribution along the normal axis for each aperture positions: (a) observation points 1 to 3, (b) observation points 3 to 11, (c) observation points 11 to 21.

moment being proportional to the tangential component of the external magnetic field. The two proportionality constants — known as electric and magnetic polarizabilities of the aperture — depend only on its shape and size. Bethe's theory assumes the external field to be uniform over the whole aperture region. Recently, [19–21] further investigated the cases of nonuniform excitations, deriving aperture polarizabilities for nonuniform incident fields.

The equivalent-dipole model, however, breaks down when the observation point is very close to the aperture — within roughly one aperture radius. For such near-field regions, an analytical theory that accurately reproduces the local field distribution is required. Fortunately, Jackson has treated this problem in detail [17]. As noted earlier, his analysis addresses the specific geometry of a circular hole in an infinite, perfectly conducting plane. Next, we further demonstrate that the electric-field distribution along the aperture axis can also be approximated by the result for an apertured infinite plane. According to Jackson's theoretical analysis for a circular aperture in an infinite conducting sheet, the magnitude of the penetrating field along the normal axis of the aperture can be easily derived, which is expressed as:

$$E_x(d) = \frac{E_a}{\pi}\left[\tan^{-1}\left(\frac{a}{d}\right) - \frac{a}{d}\frac{1}{1+(a/d)^2}\right] \tag{1}$$

wherein, E_a denotes the unperturbed field in the absence of the aperture, a the aperture radius, and d the distance from the field point to the center of the aperture. On the basis of Eq. (1), we have plotted normalized field-strength curves for the ten aperture locations and compared them with the prediction of Eq. (1),

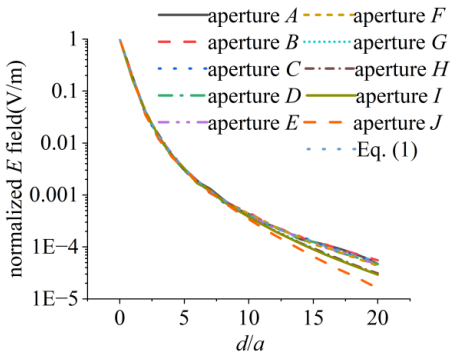

FIGURE 6. Comparison of the normalized E field distributions with Eq. (1) for the ten aperture locations.

as shown in Figure 6. It can be seen that, when the observation point is close to the aperture, all curves agree well with the analytical result given by Eq. (1). As the observation point moves farther away, the curves gradually deviate from Eq. (1), and the deviation sets in earlier for apertures located closer to the edge of the wall. Nevertheless, at these larger distances the field strength is already very weak, so its significance as an electromagnetic disturbance is negligible.

Owing to the cutoff-waveguide effect, increasing the wall thickness improves the shielding effectiveness, but this improvement is synchronous for apertures at all positions and can be approximated by $e^{-\pi t/d}$, where t is the thickness, and d is the aperture diameter [22]. Consequently, taking thickness into account does not alter the rule for selecting aperture positions. Moreover, since the thickness is generally less than 2 mm, its contribution to field attenuation is small and can be neglected from the viewpoint of improving electrostatic shielding.

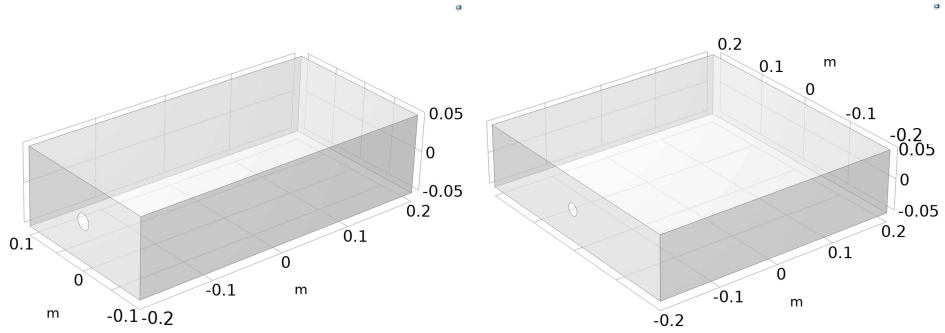

FIGURE 7. The geometries of the two additional boxes: the left (box $1^{\#}$) has the dimensions of 0.4 m × 0.4 m × 0.1 m and the right (box $2^{\#}$) has the dimensions of 0.4 m × 0.2 m × 0.1 m.

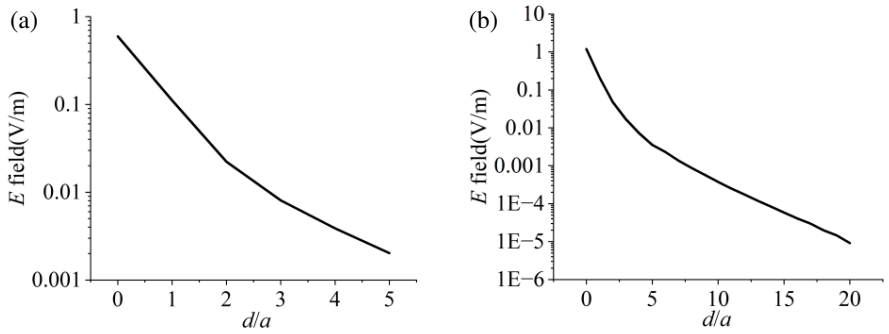

FIGURE 8. For box $1^{\#}$ (0.4 m × 0.4 m × 0.1 m), electric-field distribution along the line from the aperture center to the shielding-box center: (a) aperture at the center of the 0.4 m × 0.4 m wall; (b) aperture at the center of the 0.4 m × 0.1 m wall. In both cases, the external electric field is always perpendicular to the perforated wall.

3.4. The Choice of the Aperture Position

To minimize electric-field penetration, the aperture should be always placed at or very close to the center of the chosen wall. Moreover, if the direction of the external field is known, the aperture should be opened at the center of a side wall (i.e., a surface parallel to the electric field). Although in practice the various side walls may be not identical, the electric fields coupled into the enclosure under these conditions are all very weak, so further distinction among the side walls is unnecessary.

However, if the external field direction is unknown or may vary with time in practice, we must design for the worst-case scenario that yields the best shielding effectiveness. The worst case occurs when the apertured wall is perpendicular to the external field. For the cubic enclosure considered earlier, all faces have the same dimensions, so any face can be chosen indiscriminately. Yet for a rectangular shield of unequal edges, the question of which face to perforate — so that the penetrating field is minimized when the external field is perpendicular to that face — requires further study. Moreover, in practice rectangular shields with varying length-to-width-to-height ratios are frequently employed. To this end, we examined two additional shield geometries: box $1^{\#}$ and $2^{\#}$ have the dimensions 0.4 m × 0.4 m × 0.1 m and 0.4 m × 0.2 m × 0.1 m, respectively, as displayed in Figure 7.

For box $1^{\#}$, Figures 8(a) and 8(b) show the axial electric-field distributions when the aperture is centered on the larger wall (0.4 m × 0.4 m) and smaller wall (0.4 m × 0.1 m), respectively; the external field is always oriented perpendicular to the perforated wall. Comparing the two figures shows that, near the aperture, the field is smaller for the larger wall; near the center of the box, however, the field is smaller for the smaller wall. This arises because the field decays rapidly with the field point moving far away from the aperture. For the smaller wall, the distance from box center to the wall is the greatest, leading to the strongest attenuation.

For box $2^{\#}$, Figures 9(a), 9(b), and 9(c) show the electric-field distributions along the line from the aperture center to the box center when the aperture is located at the center of the large wall (0.4 m × 0.2 m), medium wall (0.4 m × 0.1 m), and small wall (0.2 m × 0.1 m), respectively. Note that the external electric field is always oriented perpendicular to the perforated wall. Once again, the field near the aperture is the smallest when the aperture is in the large wall, whereas the field at the center of the enclosure is the smallest when the aperture is in the small wall.

In summary, to minimize the field near the aperture one should choose the largest wall; to minimize the field at the center of the shielding box one should choose the wall perpendicular to the enclosure's longest edge.

3.5. The Coexistence Effect

In practice, multiple apertures often coexist. Here we evaluate the proximity effect between two apertures, i.e., how the penetrated field changes as the separation between the two aper-

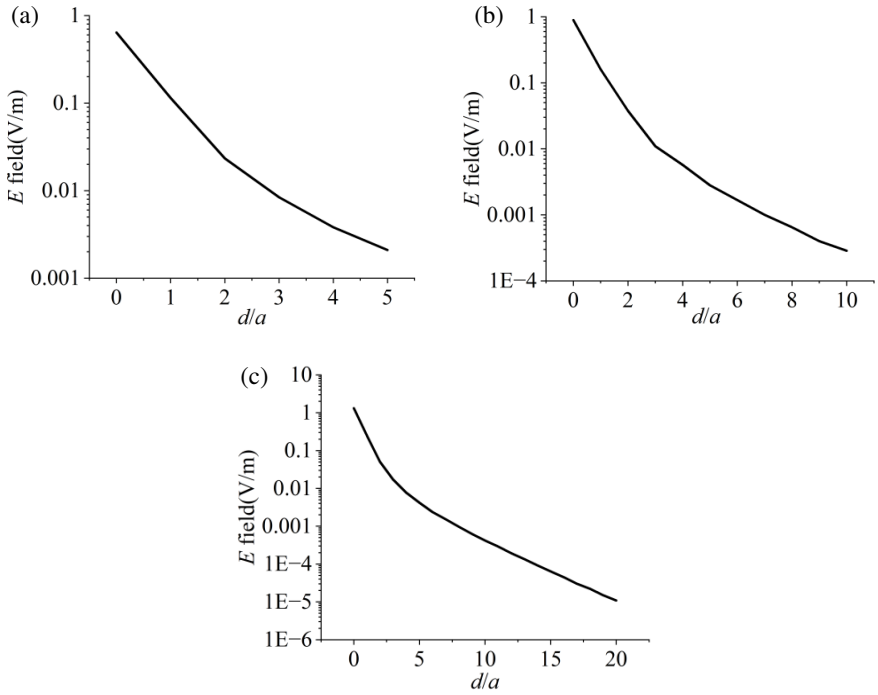

FIGURE 9. For box $2^{\#}$ (0.4 m × 0.2 m × 0.1 m), Electric-field distribution along the line from the aperture center to the box center: (a) aperture at the center of the 0.4 m × 0.4 m wall; (b) aperture at the center of the 0.4 m × 0.2 m wall; (c) aperture at the center of the 0.2 m × 0.1 m wall. In all cases, the external electric field is always perpendicular to the perforated wall.

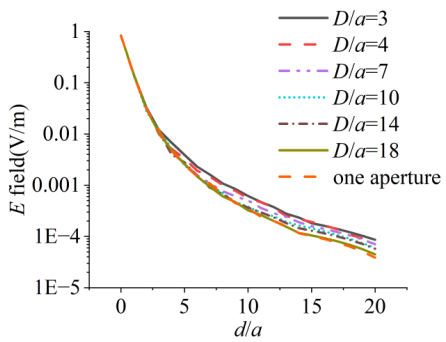

FIGURE 10. Electric field distributions on the axis of aperture 1, with both aperture 1 and aperture 2 present, for various center-to-center separations. Aperture 1 is centered on the $x = -0.2$ m wall; aperture 2 lies on the same wall. D denotes the center-to-center distance between the two apertures, a represents the aperture radius, and d/a signifies the normalized distance from the observation point to the center of aperture 1. For comparison, the result for aperture 1 alone is also shown and labeled "one aperture."

tures decreases. We assume that aperture 1 is centered on the face $x = -0.2$ m of the cube with 0.4 m sides, while aperture 2 differs from aperture 1 only in its y-coordinate, which is set to D. Consequently, the center-to-center distance between the two apertures equals D. Figure 10 plots, for several values of D, the magnitude of the field on the axis of aperture 1 versus the normalized coordinate D/a. The result for aperture 1 alone, labeled "one aperture," is also shown. When $d/a < 2.5$, all curves virtually coincide; once d/a exceeds 2.5, they begin to diverge. For field points far from the aperture, the field strength gradually decreases as D/a increases, approaching the result corresponding to "one aperture".

This behavior arises because, with both apertures present, the penetrated field can be expressed as the superposition of the fields produced by each aperture individually. Near either aperture this superposition has little effect: the local field is dominated by the aperture itself, while the contribution from the distant aperture is small. Far from both apertures, however, their distances to the observation point are comparable, so their penetrated fields are of similar strength, and the superposed result becomes noticeably larger.

4. CONCLUSIONS

For electrostatic shielding, the guidelines for selecting an aperture location on a rectangular shielding enclosure can be summarized in two steps.

(1) Choose which wall to perforate. If the direction of the external electric field is known, place the aperture on the wall that is parallel to that field. If the direction of the external electric field cannot be determined, design for the worst case: the field is perpendicular to the aperture. To minimize the field near the aperture, one should place the aperture in the wall with the largest area. If, instead, to minimize the field at the center of the enclosure, one should place the aperture in the wall that is perpendicular to the longest edge of the shielding box.

(2) Locate the aperture on the chosen wall. Once the wall is selected, position the aperture at or very near the center of that wall.

Moreover, the field distribution along the axis normal to the aperture can be well approximated by Eq. (1) provided that the aperture is not placed too close to any edge of the wall. The coexistence effect is negligible for observation points near each aperture, but is evident for observation points far from the apertures.

Actual shielding enclosures contain internal components and objects, which significantly affect the field distribution. This influence depends on factors such as material, size, geometry, and position, and deserves consideration in future research.

ACKNOWLEDGEMENT

This work is supported by the Science and Technology Project of State Grid Corporation of China (Grant 5108-202218280A-2-347-XG).

REFERENCES

[1] Celozzi, S., R. Araneo, P. Burghignoli, and G. Lovat, *Electromagnetic Shielding: Theory and Applications*, John Wiley & Sons, 2022.

[2] VijayKashimatt, M. G., M. Vatnalmath, and V. Auradi, "A review on conductive polymer composites focusing on advancements in electrical conductivity, and electromagnetic shielding capabilities," *Polymer Composites*, Review Article, 2025.

[3] Li, Z., Z. Gan, L. Ren, B. Li, P. Kong, H. Li, and J. Li, "Research on single-hole compensated passive magnetic shielding structure for electric vehicle wireless power transfer systems," *Progress In Electromagnetics Research B*, Vol. 107, 63–75, 2024.

[4] Singh, D., R. P. Yadav, and H. Joshi, "Multi-band 3D printed frequency selective surface for RF shielding applications," *Progress In Electromagnetics Research Letters*, Vol. 122, 59–65, 2024.

[5] Meka, N. and K. Shambavi, "Conformal angularly stable quad-band frequency selective surface for EMI shielding," *Progress In Electromagnetics Research Letters*, Vol. 122, 29–35, 2024.

[6] Kalantari, M. and S. H. H. Sadeghi, "An efficient surface integral equation-method of moments for analysis of electromagnetic shielding effectiveness of a perforated isotropic and lossy enclosure," *IEEE Transactions on Electromagnetic Compatibility*, Vol. 67, No. 1, 99–107, 2025.

[7] Jin, H., H. Zhang, Y. Ma, K. Chen, and X. Sun, "An analytical hybrid model for the shielding effectiveness evaluation of a dual-cavity structure with an aperture array," *Progress In Electromagnetics Research Letters*, Vol. 91, 109–116, 2020.

[8] Shen, W., S. Wang, W. Li, H. Jin, and H. Zhang, "An extended hybrid analytical model for shielding effectiveness prediction of multi-cavity structure with numerous apertures," *Progress In Electromagnetics Research M*, Vol. 96, 181–190, 2020.

[9] Bai, J., X. Li, J. Zhou, and M. Li, "Integrated prediction of condensation-corrosion-shielding effectiveness of metal box with gaps by simulations," *Progress In Electromagnetics Research C*, Vol. 144, 137–145, 2024.

[10] Boridy, E., "Penetration of electric fields into open conducting cavities," *Journal of Applied Physics*, Vol. 68, No. 9, 4385–4392, 1990.

[11] Casey, K. F., "Quasi-static electric-and magnetic-field penetration of a spherical shield through a circular aperture," *IEEE Transactions on Electromagnetic Compatibility*, Vol. 27, No. 1, 13–17, 1985.

[12] Liu, Y., B. Tang, and Y. Gao, "Electric field penetration and perturbation problems of a nonuniform cylindrical cavity with a slot," *IEEE Transactions on Electromagnetic Compatibility*, Vol. 37, No. 3, 458–462, 1995.

[13] Liu, T., A. Schnabel, L. Li, Z. Sun, and J. Voigt, "Impact of circular apertures on static shielding performances of spherical magnetic shields," *IEEE Magnetics Letters*, Vol. 11, 1–5, 2020.

[14] Hao, S.-Y., X.-P. Lou, J. Zhu, G.-W. Chen, and H.-Y. Li, "Magnetic shielding property for cylinder with circular, square, and equilateral triangle holes," *Chinese Physics B*, Vol. 30, No. 6, 060702, 2021.

[15] Yin, M.-C. and P.-A. Du, "An improved circuit model for the prediction of the shielding effectiveness and resonances of an enclosure with apertures," *IEEE Transactions on Electromagnetic Compatibility*, Vol. 58, No. 2, 448–456, 2016.

[16] "Comsol software," https://comsol.asia/comsol-multiphysics.

[17] Jackson, J. D., *Classical Electrodynamics*, 3rd ed., Chap. 3, 129–135, John Wiley & Sons, 1998.

[18] Bethe, H. A., "Theory of diffraction by small holes," *Physical Review*, Vol. 66, No. 7-8, 163, 1944.

[19] Du, Z., Z. Jiang, Z. Deng, J. Huang, and C. Jiao, "A closed-form expression of electric polarizability for elliptical apertures excited by nonuniform electric field," *Physica Scripta*, Vol. 98, No. 11, 115532, 2023.

[20] Du, Z., J. Mei, T. Li, F. Yu, H. Liu, H. Huang, T. Zhang, and C. Jiao, "Closed-form expressions for magnetic polarizabilities of circular apertures excited by nonuniform magnetic fields," *Physica Scripta*, Vol. 99, No. 12, 125545, 2024.

[21] Lu, J., Y. Shi, and C. Jiao, "The closed-form expression for the dipole moment of an elliptical aperture excited by nonuniform magnetic fields," *Physica Scripta*, Vol. 100, No. 8, 085502, 2025.

[22] Paul, C. R., R. C. Scully, and M. A. Steffka, *Introduction to Electromagnetic Compatibility*, 2nd ed., 749, John Wiley & Sons, 2006.